



Contents lists available at ScienceDirect

# Microporous and Mesoporous Materials

journal homepage: [www.elsevier.com/locate/micromeso](http://www.elsevier.com/locate/micromeso)

## Effect of catalyst loading on hydrogen storage capacity of ZIF-8/graphene oxide doped with Pt or Pd via spillover

Hu Zhou<sup>a,c</sup>, Jian Zhang<sup>b</sup>, Dong Ji<sup>b</sup>, Aihua Yuan<sup>b,\*</sup>, Xiaoping Shen<sup>c</sup><sup>a</sup> School of Material Science and Engineering, Jiangsu University of Science and Technology, Zhenjiang 212003, PR China<sup>b</sup> School of Environmental and Chemical Engineering, Jiangsu University of Science and Technology, Zhenjiang 212003, PR China<sup>c</sup> School of Chemistry and Chemical Engineering, Jiangsu University, Zhenjiang 212013, PR China

### ARTICLE INFO

#### Article history:

Received 23 January 2016

Received in revised form

20 March 2016

Accepted 7 April 2016

Available online 19 April 2016

#### Keywords:

Metal-organic framework

Graphene oxide

Platinum

Palladium

Hydrogen storage

Spillover

### ABSTRACT

In this work, a series of zeolitic imidazolate framework (ZIF-8)/graphene oxide (GO) supported Pt or Pd nanoparticles (NPs) with different loading amounts were obtained via a simple liquid impregnation of ZIF-8/GO with metal salt solution followed by a reduction treatment. Powder X-ray diffraction, Fourier transform infrared spectra, scanning electron microscopy, transmission electron microscopy, energy-dispersive X-ray spectroscopy, inductively coupled plasma-emission spectroscopy, and nitrogen adsorption-desorption measurements were employed to investigate the physical and chemical properties of as-prepared samples. The Pt and Pd particles in the corresponding composites have average diameters of about 4.5 and 4.6 nm, respectively. All metal-doped ZIF-8/GO composites maintained the host framework of pure ZIF-8, although their specific surface areas were significantly reduced. The introduction of metal catalysts into the ZIF-8/GO matrix does not favor the hydrogen adsorption performance at 77 K due to the physisorption mechanism. In contrast, the adsorption isotherms at 298 exhibited dramatically improved storage capacities, by factors of 3.8–11.8 (Pt-doped ZIF-8/GO) and 7.9–12.6 (Pd-doped ZIF-8/GO) times over pristine ZIF-8 at the hydrogen pressure of 860 mmHg. This enhancement is mainly attributed to the spillover mechanism by metal catalysts into the ZIF-8/GO support. More importantly, the effect of catalysts dispersion and content on the level of hydrogen storage was also explored, which showed that the composites with the most homogeneous metal distribution and moderate loading amount would display the highest hydrogen adsorption performance.

© 2016 Elsevier Inc. All rights reserved.

## 1. Introduction

Hydrogen storage is one of the key issues for the realization of fuel-cell powered vehicles using hydrogen as the energy carrier, and ongoing efforts have been devoted toward the development of suitable and efficient hydrogen storage materials [1,2]. Unfortunately, it has been recognized that the excellent hydrogen storage performances of these materials (i.e. various adsorbents, chemical hydrides, etc) are generally only achieved at extremely low temperatures (typically 77 K or 87 K), and dramatically decline (usually less than 1 wt%) under ambient temperatures and even 10 MPa due to the weak van der Waals interactions between hydrogen and adsorbents [3,4]. As a consequence, the adsorption amounts under

more moderate conditions must be improved from the viewpoints of automobile applications.

Early studies have confirmed that the presence of metal (Pt, Pd, Ni, etc) nanoparticles (NPs) could obviously improve the ambient-temperature hydrogen storage capacities of carbon-based materials via the spillover effect [5–7]. In fact, the hydrogen spillover phenomenon has been well known in heterogeneous catalysis and related studies have been reviewed [8]. Briefly, hydrogen spillover is typically defined as the dissociative chemisorption of hydrogen on metal NPs and subsequent migration of atomic hydrogen onto the surface of the acceptor [9,10]. Later, the spillover mechanism was successfully extended to the field of metal-organic frameworks (MOFs). MOFs, which are assembled from metal ions and organic bridging ligands, are promising candidates for hydrogen storage materials because of their low densities, high specific surface areas and porosities as well as adjustable chemical functionalities [11–15]. It was determined that the significantly enhanced ambient-temperature hydrogen uptakes have been achieved by

\* Corresponding author.

E-mail address: [aihua.yuan@just.edu.cn](mailto:aihua.yuan@just.edu.cn) (A. Yuan).

physically mixing MOFs and Pt/active carbon (AC) catalysts (or with additional bridging carbon), where hydrogen atoms moved from Pt surface to AC and then to MOFs [16,17]. For this type of adsorbents, MOFs would provide a good basis owing to the availability of a wide variety of structures and compositions, which could be utilized to systematically determine the effect of the support.

Recently, MOF hybrids with graphene oxide (GO) have been synthesized by combining the remarkable advantages of MOF and GO, and the synergistic effects between both components on the porosity and chemistry of final materials have resulted in a significant improvement in gas adsorption compared to pure MOFs [18–26]. This prompted our group to use MOF/GO hybrids instead of MOFs as supports to incorporate metal catalysts. Along this line, we have constructed several Pt-doped MOF/GO composites (MOF = HKUST-1, MIL-101 and ZIF-8), and evaluated hydrogen storage capacities at 298 K were obtained via spillover [27–30]. Furthermore, the effects of structural features of MOFs and metal doping strategies on hydrogen adsorption properties of final materials have also been documented. Specifically speaking, the crystallinities, morphologies, and texture parameters of Pt@HKUST-1/GO and Pt@MIL-101/GO composites were induced obviously by GO content. Especially, the formation of Pt@MIL-101/GO with high GO content is not favored because of the specific geometry of MIL-101. In addition, the incipient-wetness impregnation method has produced a significant aggregation of metal NPs, while the well dispersion was observed for the chemical impregnation followed by a reduction treatment.

Although encouraging progress has been achieved, the nature of factors influencing the level of hydrogen storage via spillover is still disputable due to the lack of understanding of the exact mechanism and the contrary experimental results [31]. As a result, it is necessary to further probe the role of the variables involved in the process in order to optimize the system for hydrogen storage. As a continuation of our developed metal-doped MOF/GO materials for hydrogen storage, a series of ZIF-8/GO deposited with varying Pt or Pd loading amounts were prepared here through a facile liquid impregnation method, in which  $\text{H}_2\text{PtCl}_6$  (or  $\text{PdCl}_2$ ),  $\text{NaBH}_4$  and polyvinyl alcohol (PVA) act as the metal precursors, reducing and stabilizing agents, respectively. To our knowledge, the syntheses and characterizations of Pd-doped MOF/GO hybrids were not been reported to date. The purpose of this work is to establish the influence of different dispersion degrees and contents of metal catalysts on ambient-temperature hydrogen adsorption properties of final materials, and to further elucidate the storage mechanism via spillover in the metal-doped MOF/GO system.

## 2. Experimental

### 2.1. Synthesis

All starting materials and solvents were purchased from commercial sources and used without further purification. Graphene oxide (GO) was prepared by oxidation of graphite via a modified Hummers method [32].

**ZIF-8.** ZIF-8 was synthesized according to the reported procedure [33]. Typically, a methanol solution (100 mL) of  $\text{Zn}(\text{NO}_3)_2 \cdot 6\text{H}_2\text{O}$  (4.94 mmol) was added slowly into a methanol solution (100 mL) of 2-methylimidazole (39.52 mmol) with vigorous stirring. After reacting at room temperature for 1 h, the resulting precipitations were collected by centrifugation and washed with methanol for several times. Finally, the products were dried overnight at 160 °C under vacuum.

**ZIF-8/GO.** A certain amount of GO (5 wt% of the final material weight) was dispersed in methanol (30 mL) and sonicated for 5 h. The resulted GO dispersion was added into the reaction system

during the preparation of ZIF-8. The resulting precipitations was centrifuged, washed several times with water-methanol solvent, and then dried overnight at 160 °C under vacuum with further use.

**Pt<sub>n</sub>@ZIF-8/GO and Pd<sub>n</sub>@ZIF-8/GO.** To incorporate Pt or Pd catalysts into the ZIF-8/GO support, a simple impregnation method was applied using the developed similar method reported in our previous work [27]. Taking the preparation of Pt-doped ZIF-8/GO with a low Pt loading as an example, an aqueous solution of  $\text{H}_2\text{PtCl}_6 \cdot 6\text{H}_2\text{O}$  (1 mL, 0.01 M) was first mixed with polyvinyl alcohol (PVA) (PVA monomer/metal = 10:1 M ratio, 4.41 mg) and stirred for 1 h at room temperature. 100 mg of freshly activated ZIF-8/GO sample was added to above solution, and the mixture was stirred for 2 h. Then, an aqueous solution of  $\text{NaBH}_4$  ( $\text{NaBH}_4$ /metal = 5:1 M ratio, 0.5 mL, 0.1 M) was added dropwise to the reaction mixture in an ice bath with vigorous stirring. After further stirring for 5 h, the precipitations were isolated by filtration, and washed thoroughly with deionized water/methanol. Finally, the resulting products were dried overnight at 333 K and then activated at 433 K under vacuum for 12 h. The Pt content on the sample was 0.53 wt% based on ICP analysis. The composites with varying Pt loadings of 1.95 and 5.96 wt% were also prepared by an identical protocol except for using corresponding amounts of Pt salt. To synthesize Pd-doped ZIF-8/GO composites with different Pd loadings, the salt  $\text{PdCl}_2$  were used instead of  $\text{H}_2\text{PtCl}_6$  and the other procedure was similar to that for the preparation of Pt-doped ZIF-8/GO. The Pd contents on the samples were 0.21, 1.27 and 5.75 wt%, respectively, based on ICP analysis. All as-synthesized composites are denoted as Pt<sub>n</sub>@ZIF-8/GO or Pd<sub>n</sub>@ZIF-8/GO, where n is the actual weight percentage of metal catalysts.

### 2.2. Instrumentation and measurements

Powder X-ray diffraction (XRD) measurements were performed with a Shimadzu XRD-6000 diffractometer with Cu-K $\alpha$  radiation ( $\lambda = 1.5406 \text{ \AA}$ ). Fourier transform infrared spectra (FT-IR) were collected on a Nicolet FT 1703 $\times$  spectrometer with KBr pellets in the 4000–400  $\text{cm}^{-1}$  region. The Pt or Pd contents in the samples were determined quantitatively by an Agilent 7700 inductively coupled plasma-emission spectrometry (ICP-MS). The field-emission scanning electron microscopy (FE-SEM) and high-resolution transmission electron microscopy (HR-TEM) observations were carried out using a ZEISS Merlin Compact and a JEOL JEM-2100F, respectively. The elemental mapping analysis was examined by energy-dispersive X-ray spectrometry (EDS, Oxford X-Max). The  $\text{N}_2$  and  $\text{H}_2$  adsorption-desorption isotherms were recorded on a Micrometrics ASAP 2020 instrument. The samples were outgassed under vacuum at 433 K for 24 h prior to the adsorption measurements. High-purity nitrogen and hydrogen gases (99.999%) were used for all measurements. The Brunauer–Emmett–Teller (BET) specific surface area was calculated from the adsorption data in the relative pressure  $P/P_0$  range from 0 to 0.30. Total pore volume was estimated by a single point method at the relative pressure  $P/P_0$  of 0.99. The pore diameter distribution curves were determined from the analysis of the adsorption branch of the isotherm using the Horvath-Kawazoe method.

## 3. Results and discussion

The powder XRD patterns of as-synthesized ZIF-8, ZIF-8/GO and metal-doped ZIF-8/GO samples are shown in Fig. 1. The diffraction patterns of as-prepared ZIF-8 match well with the simulated ones from single-crystal XRD structural data, indicating the high purity of products [34]. The ZIF-8/GO sample exhibits identical diffraction patterns to pristine ZIF-8 and no apparent loss of crystallinity, revealing that the incorporation of GO does not disturb the whole

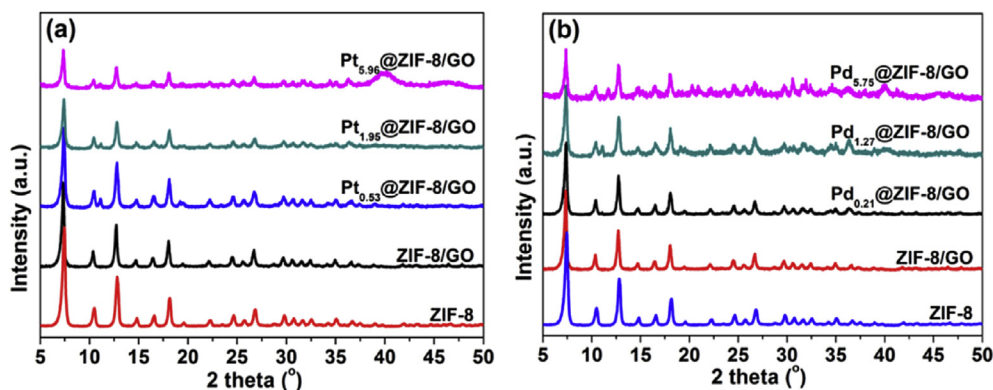


Fig. 1. Powder XRD patterns of (a)  $Pt_n@ZIF-8/GO$  and (b)  $Pd_n@ZIF-8/GO$  systems.

assembly process of MOF. The absence of characteristic diffraction peaks of GO can be ascribed to the much low content (5 wt%) or/and the exfoliation/high dispersion of GO in the composite [35]. The main diffraction peaks of all metal-doped ZIF-8 samples were almost same as those of ZIF-8 and ZIF-8/GO in diffraction angles, except a weak and broad peak was observed at around  $40.0^\circ$  and  $46.5^\circ$ , indicating the inclusion of Pt or Pd particles inside the ZIF-8/GO support. Generally, the diffraction intensity of the MOF material is stronger than that of nanocrystals by several orders of magnitude; thus the diffraction peaks attributed to metal nanocrystals can rarely be observed for hetero-nanostructures. In our case, especially for  $Pt_{0.53}@ZIF-8/GO$  and  $Pd_{0.21}@ZIF-8/GO$  composites, no clear characteristic diffraction peaks at around  $2\theta = 40.0^\circ$  and  $46.5^\circ$  assigned to the (111) and (200) crystal facets, respectively, of metallic Pt or Pd species are detected, which was caused by the much low contents or/and high dispersion of metal catalysts with small sizes in these composites. Nevertheless, the intensities of diffraction peaks of metallic Pt or Pd increased with increasing NPs contents in composites. Especially, the diffraction peaks of metal species for  $Pt_{5.96}@ZIF-8/GO$  and  $Pd_{5.75}@ZIF-8/GO$  samples can be clearly observed as a result of the high loadings or/and apparent agglomeration of metal NPs in the ZIF-8/GO support. The broad peaks of metal species could be attributed to the nanoscale dimension. These results have been further confirmed by morphology observations and EDS mapping analyses (see below). In addition, the whole diffraction intensities for both cases decreased slightly with respect to the ZIF-8/GO support, due to the loss in the crystallinity and/or structural distorted caused by the

incorporation of high-loading Pt or Pd particles into the ZIF-8/GO network.

FT-IR spectra of  $Pt_n@ZIF-8/GO$  and  $Pd_n@ZIF-8/GO$  systems are described in Fig. 2. The lattice vibrations of as-prepared ZIF-8 are in agreement with the fingerprint groups [19,36]. Briefly, the adsorption bands at around  $1584\text{ cm}^{-1}$  are associated with the C=N stretching vibrations of the imidazole, whereas the entire ring stretching appears as the intense and convoluted bands at  $1500\text{--}1350\text{ cm}^{-1}$ . Additionally, the in-plane and out-of-plane bending of the ring are observed in the region of  $1350\text{--}900\text{ cm}^{-1}$  and below  $800\text{ cm}^{-1}$ , respectively. Notably, the characteristic bands of GO were not detected in the ZIF-8/GO and metal-doped ZIF-8/GO samples due to the much low contents of GO component. The ZIF-8/GO support exhibits identical bands to pure ZIF-8, suggesting that the immobilizing of GO did not disturbed the coordination of 2-methylimidazole linker to the zinc(II) centers and thus the formation of MOF, as confirmed by powder XRD analysis. No obvious changes in adsorption wavenumbers and intensities for the composites with low and moderate metal loadings were observed with respect to ZIF-8 and ZIF-8/GO. However, the significantly decreased intensities were found for the  $Pt_{5.96}@ZIF-8/GO$  and  $Pd_{5.75}@ZIF-8/GO$  composites with high catalyst contents, indicating the poor crystallinities of both samples. Above analysis supports the results drawn from XRD experiments.

The morphologies of all samples were investigated by SEM and TEM images (Figs. 3 and 4). As shown in Fig. 3a and b, GO was observed as crumpled layered structure, whereas ZIF-8 particles exhibit nanoscale size. ZIF-8 nanocrystals in ZIF-8/GO are randomly

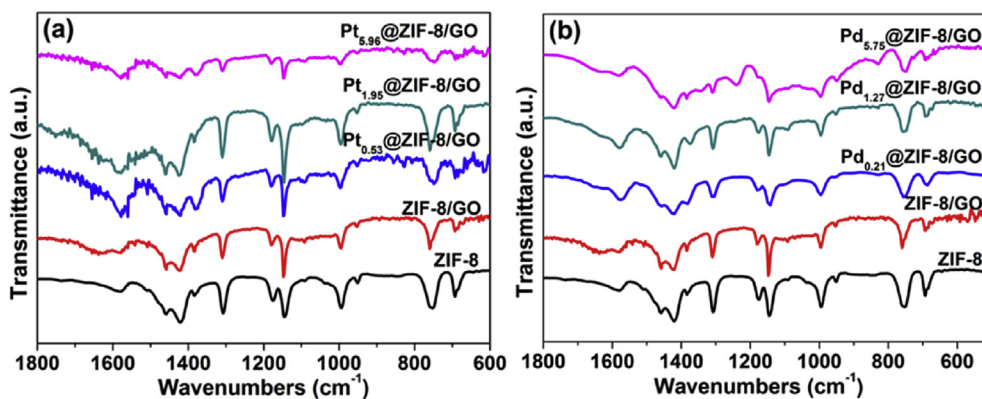
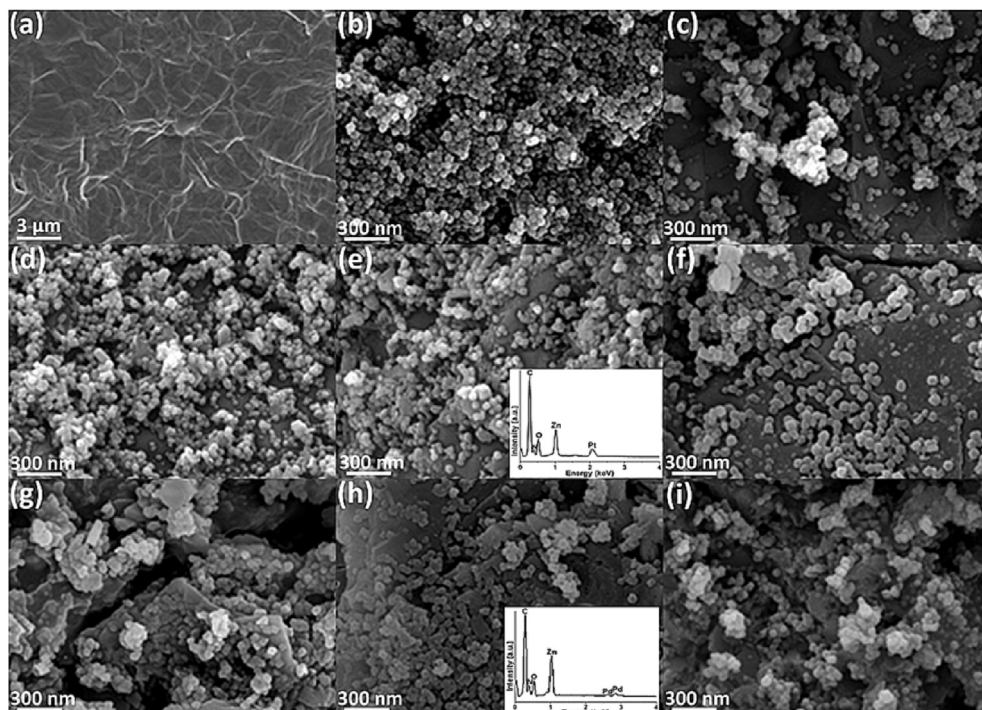
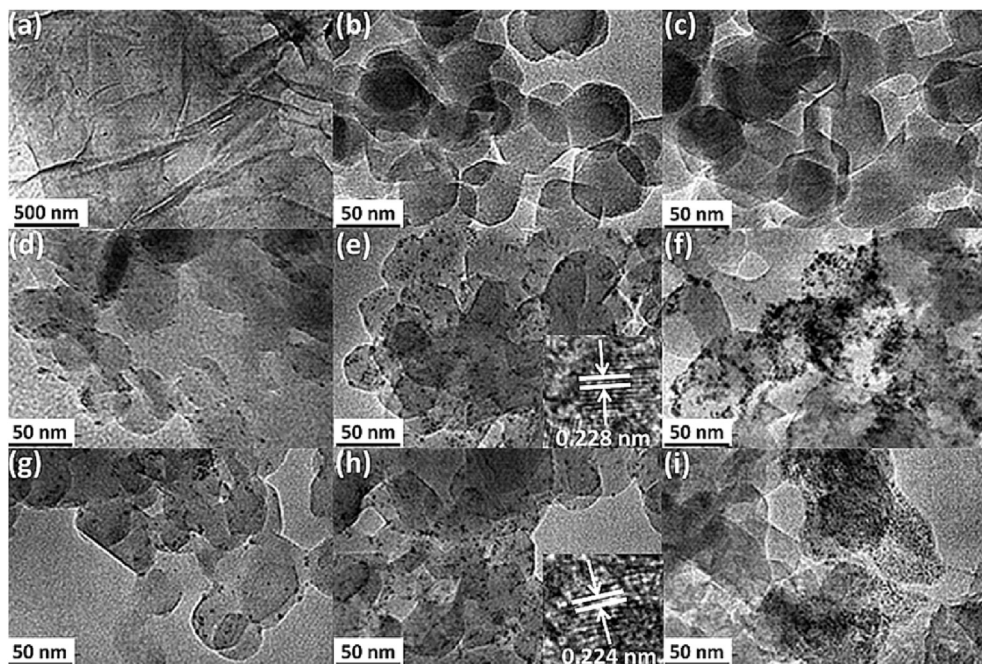


Fig. 2. FT-IR spectra of (a)  $Pt_n@ZIF-8/GO$  and (b)  $Pd_n@ZIF-8/GO$  systems.



**Fig. 3.** SEM images of (a) GO, (b) ZIF-8, (c) ZIF-8/GO, (d) Pt<sub>0.53</sub>@ZIF-8/GO, (e) Pt<sub>1.95</sub>@ZIF-8/GO, (f) Pt<sub>5.96</sub>@ZIF-8/GO, (g) Pd<sub>0.21</sub>@ZIF-8/GO, (h) Pd<sub>1.27</sub>@ZIF-8/GO and (i) Pd<sub>5.75</sub>@ZIF-8/GO samples. Inset in (e) and (h) is the EDS patterns of Pt<sub>1.95</sub>@ZIF-8/GO and Pd<sub>1.27</sub>@ZIF-8/GO composites, respectively.



**Fig. 4.** TEM images of (a) GO, (b) ZIF-8, (c) ZIF-8/GO, (d) Pt<sub>0.53</sub>@ZIF-8/GO, (e) Pt<sub>1.95</sub>@ZIF-8/GO, (f) Pt<sub>5.96</sub>@ZIF-8/GO, (g) Pd<sub>0.21</sub>@ZIF-8/GO, (h) Pd<sub>1.27</sub>@ZIF-8/GO and (i) Pd<sub>5.75</sub>@ZIF-8/GO samples. Inset in (e) and (h) is the HR-TEM images of Pt and Pd nanoparticles in Pt<sub>1.95</sub>@ZIF-8/GO and Pd<sub>1.27</sub>@ZIF-8/GO composites, respectively.

anchored and dispersed on GO sheets, and no significant changes in the morphology for ZIF-8 occurred upon the material preparation (Fig. 3c). EDS results at various points for metal-doped ZIF-8/GO composites indicated the similar composition results and the presence of Pt or Pd elements, although metal particles cannot be observed from SEM images because of their very small sizes (Fig. 3d–i). What is more, elemental mapping analysis revealed

that Pt or Pd NPs are homogeneously dispersed into the whole ZIF-8/GO network when catalyst loadings are relatively low and moderate. However, noticeable aggregations were observed for Pt<sub>5.96</sub>@ZIF-8/GO and Pd<sub>5.75</sub>@ZIF-8/GO composites with high metal contents (Figs. S2–S7). This result is in good agreement with above XRD observations, where noticeable diffraction peaks assigned to metal species appeared for both cases.

The morphologies of these nanoscale materials are further investigated from TEM images. As shown in Fig. 4a and b. GO has typical wrinkled sheets, whereas ZIF-8 nanocrystals mostly present as regular hexagonal morphologies and uniform size of about 50 nm. The shapes of ZIF-8 particles changed slightly for metal-doped ZIF-8/GO composites (Fig. 4c). In the case of samples with low and moderate metal loadings (Fig. 4d, e, g, h), hexagons with a few irregular squares or rectangles are seen. Upon further increasing catalyst loadings ( $\text{Pt}_{5.96}\text{@ZIF-8/GO}$ ,  $\text{Pd}_{5.75}\text{@ZIF-8/GO}$ ) (Fig. 4f, i), some particles transform to irregular spherical shape. So, the morphologies of ZIF-8 in composites are tuned slightly by the percentage of metal species. The high-resolution TEM images show that Pt and Pd particles in  $\text{Pt}_{1.95}\text{@ZIF-8/GO}$  and  $\text{Pd}_{1.27}\text{@ZIF-8/GO}$  composites have average diameters of ca. 4.5 and 4.6 nm as estimated, respectively (Fig. S8, Fig. S9). Thus, these metal species can hardly access into the pore channels of ZIF-8, because the particle sizes are much bigger than the pore sizes (1.16 nm, 0.34 nm) of ZIF-8 [34]. They are mainly located at the surface and edges, as in the case of metal NPs located on MOF-5, ZIF-8, and MIL-101 materials [37–39]. High-resolution TEM images of a Pt or Pd particle are shown in the inset of Fig. 4e, h, from which well-defined lattice fringes with the spacing of 0.228 nm or 0.224 nm can be obviously observed, corresponding to face-centered cubic Pt(111) and Pd(111) planes, respectively. The metals NPs are uniformly dispersed in the wide range on the external surface and edges of the ZIF-8/GO support without any aggregation for  $\text{Pt}_{1.95}\text{@ZIF-8/GO}$  and  $\text{Pd}_{1.27}\text{@ZIF-8/GO}$  composites at moderate catalyst loadings, while a few metal particles were found in  $\text{Pt}_{0.53}\text{@ZIF-8/GO}$  and  $\text{Pd}_{0.21}\text{@ZIF-8/GO}$  because of the low catalyst contents. However, it should be mentioned here that there are severe catalyst aggregations forming large islands in the case of high loadings ( $\text{Pt}_{5.96}\text{@ZIF-8/GO}$ ,  $\text{Pd}_{5.75}\text{@ZIF-8/GO}$ ) (Fig. 4f and i), as confirmed by XRD and EDS results (Figs. 4 and 7). In fact, the different catalyst loadings may be

responsible for the nitrogen and hydrogen adsorption properties of such composite system (see below).

The  $\text{N}_2$  physisorption isotherms (Fig. 5) of as-synthesized ZIF-8, ZIF-8/GO and metal-doped ZIF-8/GO are all of type-I [40], characteristic of microporous materials, and the textural parameters are summarized in Table 1. This proves that ZIF-8 is robust enough to maintain its crystal and pore structure during the loading process of GO and metal components. Also, the mild conditions provided by the simple liquid impregnation followed by a reduction treatment are important for the intactness of the ZIF-8/GO support after metal loading. As shown in Fig. 5, ZIF-8 has a BET-specific surface area of  $1297 \text{ m}^2 \text{ g}^{-1}$ , close to the published values [41–43]. The steep increase in the adsorbed amount at low relative pressure reveals the presence of microporosity in the sample. It should be noted that the BET value ( $1247 \text{ m}^2 \text{ g}^{-1}$ ) measured for ZIF-8/GO is slightly higher than the hypothetical one ( $1232 \text{ m}^2 \text{ g}^{-1}$ ) calculated by physically mixing the GO and ZIF-8 components. This can be reasonably attributed to the synergistic effect between GO and MOF components, where new pores were formed at the interface between GO layers and MOF, as observed in other MOF/GO hybrids [19,22,25]. More generally, the formation of these new pores can also be confirmed by the slight increase of pore volumes from  $1.225 \text{ cm}^3 \text{ g}^{-1}$  (ZIF-8) to  $1.281 \text{ cm}^3 \text{ g}^{-1}$  (ZIF-8/GO). In comparison with ZIF-8 and ZIF-8/GO, the BET values and pore volumes of metal-doped ZIF-8/GO composites decreased with increasing metal NPs contents in the ZIF-8/GO support. Considering the much larger particle sizes of catalysts than the cavity of the host ZIF-8 framework determined by TEM results, these metal NPs are not encapsulated in the cages of ZIF-8 but located at the surface and edges of pores. This fact has been further demonstrated by the pore diameter distribution. As shown in Fig. 6, the incorporation of GO and catalysts does not alter the pore size, while the intensities gradually decreased upon the increasing of metal loading. The decrease of

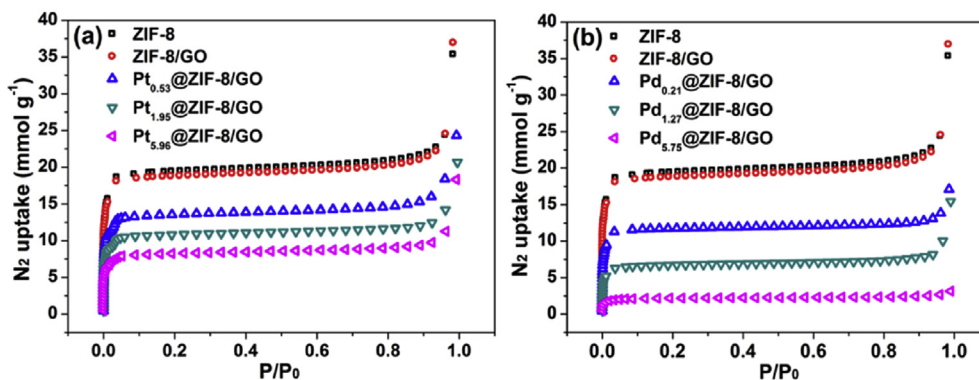


Fig. 5. Nitrogen adsorption isotherms of (a)  $\text{Pt}_n\text{@ZIF-8/GO}$  and (b)  $\text{Pd}_n\text{@ZIF-8/GO}$  systems at 77 K.

Table 1

Specific surface areas, pore volumes, and hydrogen uptakes at 298 K for  $\text{Pt}_n\text{@ZIF-8/GO}$  and  $\text{Pd}_n\text{@ZIF-8/GO}$  systems.

Sample	NPs loadings (wt%)	$S_{\text{BET}}^a$ ( $\text{m}^2 \text{ g}^{-1}$ )	$V_{\text{total}}^b$ ( $\text{cm}^3 \text{ g}^{-1}$ )	$\text{H}_2$ uptake (298 K, 860 mmHg) ( $\text{mmol g}^{-1}$ )
ZIF-8	0	1297	1.225	0.036
ZIF-8/GO	0	1247	1.281	0.034
$\text{Pt}_{0.53}\text{@ZIF-8/GO}$	0.53	1008	0.843	0.135
$\text{Pt}_{1.95}\text{@ZIF-8/GO}$	1.95	804	0.717	0.424
$\text{Pt}_{5.96}\text{@ZIF-8/GO}$	5.96	612	0.635	0.206
$\text{Pd}_{0.21}\text{@ZIF-8/GO}$	0.21	793	0.593	0.311
$\text{Pd}_{1.27}\text{@ZIF-8/GO}$	1.27	462	0.535	0.453
$\text{Pd}_{5.75}\text{@ZIF-8/GO}$	5.75	160	0.109	0.283

<sup>a</sup>  $S_{\text{BET}}$  is the BET specific surface area.

<sup>b</sup>  $V_{\text{total}}$  is the total pore volume calculated from single point adsorption data.

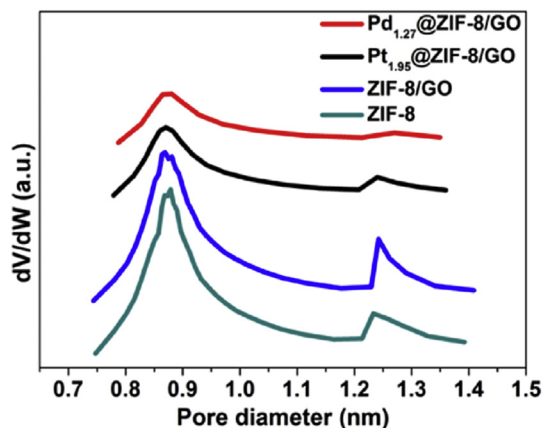


Fig. 6. The pore diameter distribution of ZIF-8, ZIF-8/GO, Pt<sub>1.95</sub>@ZIF-8/GO and Pd<sub>1.27</sub>@ZIF-8/GO samples.

intensities was caused by the appreciable loss of surface areas and porosities for these metal-doped composites, which is expected because of the blockage of cavities of ZIF-8 framework by Pt or Pd NPs, as found in the case of metal-loaded to other MOFs (MIL-101, MOF-5, MIL-53, HKUST-1, MOF-177, ZIF-8, etc.) [44,45].

The hydrogen adsorption isotherms of all samples measured at 298 K and 77 K are shown in Fig. 7 and Fig. S10, respectively. At 298 K ZIF-8 exhibited a hydrogen uptake of 0.036 mmol g<sup>-1</sup> at 860 mmHg, while a negligible change in the adsorption capacity (0.034 mmol g<sup>-1</sup>) was observed for the ZIF-8/GO support. It is interesting to note that the incorporation of Pt or Pd NPs produced a dramatic increase in hydrogen storage capacities of all composites with respect to pristine ZIF-8, by factors of 3.8–11.8 and 7.9–12.6 for Pt<sub>n</sub>@ZIF-8/GO and Pd<sub>n</sub>@ZIF-8/GO systems, respectively. It is apparent that the improved performance at 298 K cannot be ascribed to the difference in specific surface areas because of the significant loss in BET values for all metal-doped ZIF-8/GO samples compared to ZIF-8. In fact, it can be reasonably attributed to the occurrence of hydrogen transfer, so called hydrogen spillover, as already confirmed in metal supported on carbon-based materials such as carbon nanotubes [46,47], active carbon [48–53], graphene [54,55], and graphite nanofibers [56]. In order to clarify the increase in hydrogen uptake, the contribution of metal catalysts and ZIF-8/GO support were considered. On one hand, this improvement can be mainly ascribed to the high catalytic efficiency of Pt or Pd NPs on dihydrogen at ambient temperature. In our composite system, the spillover mechanism may promote the dissociation of molecular hydrogen on the surface of Pt or Pd NPs and a further diffusion of monatomic hydrogen to the porosity of ZIF-8/GO network, where

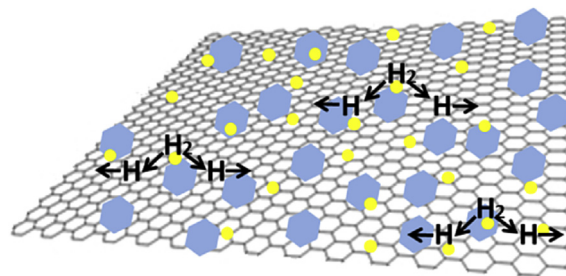


Fig. 8. The hydrogen spillover mechanism in our metal-doped ZIF-8/GO system. Blue hexagons and yellow balls represent ZIF-8 and metal (Pt or Pd) NPs, respectively. (For interpretation of the references to color in this figure legend, the reader is referred to the web version of this article.)

hydrogen atoms are chemically bounded (Fig. 8). It is claimed that the hydrogen chemisorbs onto metal NPs along with the formation of metal hybrids, which increased hydrogen adsorption amounts under ambient conditions [57,58]. On the other hand, the oxygen functional groups on GO sheets, the large surface area of ZIF-8 as well as the synergistic effect between ZIF-8 and GO components also facilitate the anchoring and dispersion of catalysts on the ZIF-8/GO support. The role of oxygen groups from the receptor in improving hydrogen adsorption amount via spillover has been documented previously on many occasions [59–63]. So the contribution for the spillover hydrogen adsorption onto the surface of GO could not be ignored in spite of slight weight ratio of GO to MOF. Above analysis indicated that the chemical properties have a considerable influence on the final hydrogen storage capacity of the present adsorbents. In addition, one of the significant observations of this study is that both Pt<sub>1.95</sub>@ZIF-8/GO (0.424 mmol g<sup>-1</sup>) and Pd<sub>1.27</sub>@ZIF-8/GO (0.453 mmol g<sup>-1</sup>) samples among all composites displayed the highest hydrogen storage capacities, 11.8 and 12.6 times larger than that of bare ZIF-8 at 298 K, respectively. The achieved best level of hydrogen storage was probably due to the homogeneous dispersion and appropriate loading of metal NPs in the support, which undoubtedly favored the interactions between metal NPs and ZIF-8/GO support. Noteworthy is the fact that the spillover effects for Pt<sub>0.53</sub>@ZIF-8/GO and Pd<sub>0.21</sub>@ZIF-8/GO samples are less obvious than those observed in Pt<sub>1.95</sub>@ZIF-8/GO and Pd<sub>1.27</sub>@ZIF-8/GO owing to the much lower contents of catalysts. Nevertheless, Pt or Pd NPs tend to be aggregated mediated by increased inter-atoms coupling if much higher contents are introduced [64]. In this case, some of metal NPs will not interact with the support and thereby the inactivity of NPs will be partially detrimental to hydrogen spillover. Regarding the Pt<sub>5.96</sub>@ZIF-8/GO (0.206 mmol g<sup>-1</sup>) and Pd<sub>5.75</sub>@ZIF-8/GO (0.283 mmol g<sup>-1</sup>) samples, the much lower surface areas caused by the incorporation of excess

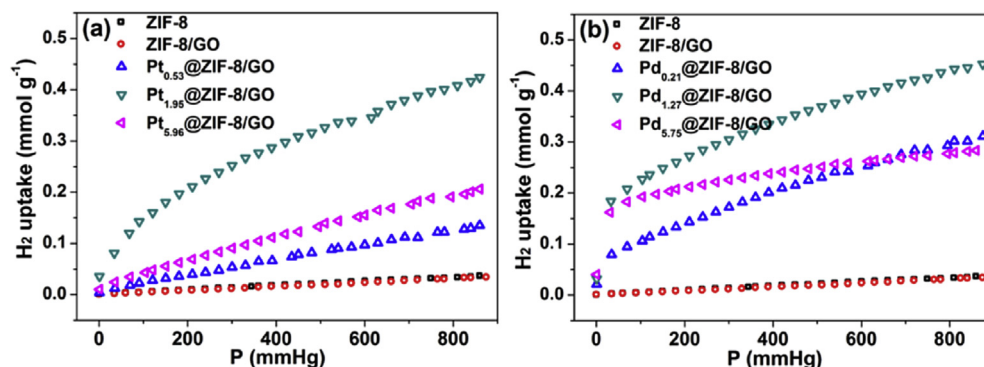


Fig. 7. Hydrogen adsorption isotherms of (a) Pt<sub>n</sub>@ZIF-8/GO and (b) Pd<sub>n</sub>@ZIF-8/GO systems at 298 K.

metal NPs and the occurrence of severe catalyst aggregation reduced efficient hydrogen adsorption. Therefore, the hydrogen storage capacity of metal-doped ZIF-8/GO systems is influenced by the loading amounts of catalysts. An important concern is that the capacities of both composites are still much higher than that of ZIF-8, similar to the result observed in Pt@MOF/GO (MOF = HKUST-1, ZIF-8), where the spillover effect was still involved despite obvious aggregations of Pt NPs throughout the MOF/GO network [28]. Above results indicated that the high dispersion and moderate catalyst loading could efficiently facilitate spillover process on adsorbents and in turn favor a pronounced increase in storage capacity at evaluated temperature.

Another important feature of this study is the hydrogen adsorption nature of all composites at extremely low temperatures. At 77 K, ZIF-8 has a hydrogen uptake of 6.92 mmol g<sup>-1</sup> at 860 mmHg, slightly higher than the reported values under the similar condition [34,65]. Notably, the storage capacities of all metal-doped ZIF-8/GO samples gradually decreased relative to that of ZIF-8 along with increasing catalysts contents (Fig. S10). At this temperature, the hydrogen uptake via spillover by metal NPs is very unlikely mainly for kinetic reasons. The amount of adsorbed hydrogen on the samples was related to the surface area of the adsorbents because the main adsorption mechanism is physisorption. Therefore, the presence of metallic NPs is useless and moreover it diminishes the hydrogen storage ability by increasing the overall weight of the material and by decreasing the microporous volume as confirmed by BET values.

#### 4. Conclusion

To summarize, ZIF-8/GO decorated by varying Pt or Pd loadings were obtained through a facile liquid impregnation approach. Interestingly, the incorporation of metal NPs led to a large improvement in the ambient-temperature hydrogen storage capacity relative to pure ZIF-8, by factors of 3.8–11.8 and 7.9–12.6 for Pt<sub>n</sub>@ZIF-8/GO and Pd<sub>n</sub>@ZIF-8/GO systems, respectively. It was found that the catalyst distribution and loading amount has a noticeable influence on the storage performance of final materials. It is worth pointing out that the composites with the most homogeneous catalyst distribution and moderate loading seem to display the highest storage capacity. In general, the more intimate contact and greater interactions between metal NPs and support will produce a stronger activation of adsorbents through the spillover effect, thereby increasing the hydrogen storage capacity under moderate conditions. Our results provide detailed insights of the hydrogen adsorption mechanism via spillover by metal catalysts, and demonstrate the feasibility of metal-doped MOF/GO as a potentially practical candidate for hydrogen storage.

#### Acknowledgments

The authors appreciate the financial supports provided by the National Natural Science Foundation (51102119, 51272095), Natural Science Foundation of Jiangsu Province (BK20151328), Qing Lan Project of Jiangsu Province, the project of the Priority Academic Program Development of Jiangsu Higher Education Institutions, China Postdoctoral Science Foundation (2014M561578) and Jiangsu Planned Projects for Postdoctoral Research Funds (1401109C).

#### Appendix A. Supplementary data

Supplementary data related to this article can be found at <http://dx.doi.org/10.1016/j.micromeso.2016.04.007>.

#### References

- [1] Y.H. Hu, *Int. J. Energ. Res.* 37 (2013) 683–685.
- [2] L. Schlapbach, A. Züttel, *Nature* 414 (2001) 353–358.
- [3] S. McWhorter, C. Read, G. Ordaz, N. Stetson, *Curr. Opin. Solid. St. M.* 15 (2011) 29–38.
- [4] K.L. Lim, H. Kazemian, Z. Yaakob, W.R.W. Daud, *Chem. Eng. Technol.* 33 (2010) 213–226.
- [5] L.F. Wang, A.J. Lachawiec Jr., R.T. Yang, *RSC Adv.* 3 (2013) 23935–23952.
- [6] L.F. Wang, R.T. Yang, *Catal. Rev.* 52 (2010) 411–461.
- [7] L.F. Wang, R.T. Yang, *Energ. Environ. Sci.* 1 (2008) 268–279.
- [8] W.C. Conner Jr., J.L. Falconer, *Chem. Rev.* 95 (1995) 759–788.
- [9] S.T. Srinivas, P.K. Rao, *J. Catal.* 148 (1994) 470–477.
- [10] A.J. Robell, E.V. Ballou, M. Boudart, *J. Phys. Chem.* 68 (1964) 2748–2753.
- [11] H. Furukawa, K.E. Cordova, M. O’Keeffe, O.M. Yaghi, *Science* 341 (2013) 1230–1235.
- [12] M.P. Suh, H.J. Park, T.K. Prasada, D.W. Lim, *Chem. Rev.* 12 (2012) 782–835.
- [13] A.H. Yuan, H. Zhou, G.W. Diao, P.D. Southon, C.J. Kepert, L. Liu, *Int. J. Hydrogen Energ.* 39 (2014) 884–889.
- [14] Y. Zhang, Y. Wang, X.F. Yan, X.Q. Liu, H. Zhou, A.H. Yuan, *Micropor. Mesopor. Mat.* 134 (2014) 15–20.
- [15] J. Wang, Y. Zhang, X.Q. Liu, J. Xiao, H. Zhou, A.H. Yuan, *Micropor. Mesopor. Mat.* 159 (2012) 100–104.
- [16] Y.W. Li, R.T. Yang, *J. Am. Chem. Soc.* 128 (2006) 8136–8137.
- [17] Y.W. Li, R.T. Yang, *J. Am. Chem. Soc.* 128 (2006) 726–727.
- [18] Y. Zhang, G. Li, H. Lu, Q. Lv, Z.G. Sun, *RSC Adv.* 4 (2014) 7594–7600.
- [19] R. Kumar, K. Jayaramulu, T.K. Maji, C.N.R. Rao, *Chem. Commun.* 49 (2013) 4947–4949.
- [20] I. Ahmed, N.A. Khan, S.H. Jhung, *Inorg. Chem.* 52 (2013) 14155–14161.
- [21] S.L. Zhang, Z. Du, G.K. Li, *Talanta* 115 (2013) 32–39.
- [22] C. Petit, J. Burrell, T.J. Bandosz, *Carbon* 49 (2011) 563–572.
- [23] C. Petit, T.J. Bandosz, *Adv. Funct. Mater.* 21 (2011) 2108–2117.
- [24] M. Jahan, Q.L. Bao, J.X. Yang, K.P. Loh, *J. Am. Chem. Soc.* 132 (2010) 14487–14495.
- [25] C. Petit, T.J. Bandosz, *Adv. Mater.* 21 (2009) 4753–4757.
- [26] X.Q. Liu, H. Zhou, Y. Zhang, Y.J. Liu, A.H. Yuan, *Chin. J. Chem.* 30 (2010) 2563–2566.
- [27] H. Zhou, J. Zhang, J. Zhang, X.F. Yan, X.P. Shen, A.H. Yuan, *Int. J. Hydrogen Energ.* 40 (2015) 12275–12285.
- [28] H. Zhou, J. Zhang, J. Zhang, X.F. Yan, X.P. Shen, A.H. Yuan, *Inorg. Chem. Commun.* 54 (2015) 54–56.
- [29] H. Zhou, X.Q. Liu, J. Zhang, X.F. Yan, Y.J. Liu, A.H. Yuan, *Int. J. Hydrogen Energ.* 39 (2014) 2160–2167.
- [30] J. Zhang, X.Q. Liu, H. Zhou, X.F. Yan, Y.J. Liu, A.H. Yuan, *RSC Adv.* 4 (2014) 28908–28913.
- [31] R. Prins, *Chem. Rev.* 112 (2012) 2714–2738.
- [32] W.S. Hummers, R.E. Offeman, *J. Am. Chem. Soc.* 80 (1958) 1339.
- [33] J. Cravillon, S. Münzer, S.J. Lohmeier, A. Feldhoff, K. Huber, M. Wiebcke, *Chem. Mater.* 21 (2009) 1410–1412.
- [34] K.S. Park, Z. Ni, A.P. Côté, J.Y. Choi, R. Huang, F.J. Uribe-Romo, H.K. Chae, M. O’Keeffe, O.M. Yaghi, *P. Natl. Acad. Sci. U. S. A.* 103 (2006) 10186–10191.
- [35] D.Y. Cai, M. Song, *J. Mater. Chem.* 17 (2007) 3678–3680.
- [36] Y. Hu, H. Kazemian, S. Rohani, Y.N. Huang, Y. Song, *Chem. Commun.* 47 (2011) 12694–12696.
- [37] H.L. Jiang, T. Akita, T. Ishida, M. Haruta, Q. Xu, *J. Am. Chem. Soc.* 133 (2011) 1304–1306.
- [38] S.X. Gao, N. Zhao, M.H. Shu, S.N. Che, *Appl. Catal. A* 388 (2010) 196–201.
- [39] M.S. El-Shall, V. Abdelsayed, A.E.R.S. Khder, H.M.A. Hassan, H.M. El-Kaderi, T.E. Reich, *J. Mater. Chem.* 19 (2009) 7625–7631.
- [40] S. Brunauer, L.S. Deming, W.R. Deming, E. Teller, *J. Am. Chem. Soc.* 62 (1940) 1723–1732.
- [41] T.T. Dang, Y.H. Zhu, J.S.Y. Ngiam, S.C. Ghosh, A. Chen, A.M. Seayad, *ACS Catal.* 3 (2013) 1406–1410.
- [42] L.H. Wee, N. Janssens, S.P. Sree, C. Wiktor, E. Gobechiya, R.A. Fischer, C.E.A. Kirschhock, J.A. Martens, *Nanoscale* 6 (2014) 2056–2060.
- [43] P. Wang, J. Zhao, X.B. Li, Y. Yang, Q.H. Yang, C. Li, *Chem. Commun.* 49 (2013) 3330–3332.
- [44] C. Rosler, R.A. Fischer, *Cryst. Eng. Comm.* 17 (2015) 199–217.
- [45] H.R. Moon, D.W. Lim, M.P. Suh, *Chem. Soc. Rev.* 42 (2013) 1807–1824.
- [46] R. Bhowmick, S. Rajasekaran, D. Friebel, C. Beasley, L.Y. Jiao, H. Ogasawara, H.J. Dai, B. Clemens, A. Nilsson, *J. Am. Chem. Soc.* 133 (2011) 5580–5586.
- [47] R. Zacharia, S. Rather, S.W. Hwang, K.S. Nahm, *Chem. Phys. Lett.* 434 (2007) 286–291.
- [48] Z. Geng, D.B. Wang, C.M. Zhang, X.Y. Zhou, H.F. Xin, X.P. Liu, M. Cai, *Int. J. Hydrogen Energ.* 39 (2014) 13643–13649.
- [49] C.S. Tsao, Y.R. Tzeng, M.S. Yu, C.Y. Wang, H.H. Tseng, T.Y. Chung, H.C. Wu, T. Yamamoto, K. Kaneko, S.H. Chen, *J. Phys. Chem. Lett.* 1 (2010) 1060–1063.
- [50] V.V. Bhat, C.I. Contescu, N.C. Gallego, *Nanotechnology* 20 (2009) 204011.
- [51] D. Saha, S.G. Deng, *Langmuir* 25 (2009) 12550–12560.
- [52] L.F. Wang, R.T. Yang, *J. Phys. Chem. C* 112 (2008) 12486–12494.
- [53] R. Campesi, F. Cuevas, R. Gadiou, E. Leroy, M. Hirscher, C. Vix-Guterl, M. Latroche, *Carbon* 46 (2008) 206–214.
- [54] P. Divya, S. Ramaprabhu, *Phys. Chem. Chem. Phys.* 16 (2014) 26725–26729.

- [55] C.H. Chen, T.Y. Chung, C.C. Shen, M.S. Yu, C.S. Tsao, G.N. Shi, C.C. Huang, M.D. Ger, W.L. Lee, *Int. J. Hydrogen Energ.* 38 (2013) 3681–3688.
- [56] B.J. Kim, Y.S. Lee, S.J. Park, *J. Colloid. Interf. Sci.* 318 (2008) 530–533.
- [57] C. Zlotea, R. Campesi, F. Cuevas, E. Leroy, P. Dibandjo, C. Volkringer, T. Loiseau, G. Férey, M. Latroche, *J. Am. Chem. Soc.* 132 (2010) 2991–2997.
- [58] R. Zacharia, S. Rather, S.W. Hwang, K.S. Nahm, *Chem. Phys. Lett.* 434 (2007) 286–291.
- [59] T.Y. Chung, C.S. Tsao, H.P. Tseng, C.H. Chen, M.S. Yu, *J. Coll. Interf. Sci.* 441 (2015) 98–105.
- [60] C.H. Chen, T.Y. Chung, C.C. Shen, M.S. Yu, C.S. Tsao, G.N. Shi, C.C. Huang, M.D. Ger, W.L. Lee, *Int. J. Hydrogen Energ.* 38 (2013) 3681–3688.
- [61] Q. Li, A.D. Lueking, *J. Phys. Chem. C* 115 (2011) 4273–4282.
- [62] Z. Wang, F.H. Yang, R.T. Yang, *J. Phys. Chem. C* 114 (2010) 1601–1609.
- [63] G.M. Psofogiannakis, G.E. Froudakis, *J. Am. Chem. Soc.* 131 (2009) 15133–15135.
- [64] S. Dag, Y. Ozturk, S. Ciraci, T. Yildirim, *Phys. Rev. B* 72 (2005) 155404.
- [65] W. Zhou, H. Wu, M.R. Hartman, T. Yildirim, *J. Phys. Chem. C* 111 (2007) 16131–16137.